ANL-ART-239
ANL-METL-34

Flow Sensor Test Article (F-STAr) – Status Report for FY2021

Nuclear Engineering Division

About Argonne National Laboratory

Argonne is a U.S. Department of Energy laboratory managed by UChicago Argonne, LLC under contract DE-AC02-06CH11357. The Laboratory's main facility is outside Chicago, at 9700 South Cass Avenue, Argonne, Illinois 60439. For information about Argonne, see http://www.anl.gov.

Disclaimer

ANL-ART-239
ANL-METL-34

Flow Sensor Test Article (F-STAr) – Status Report for FY2021

J. Rein, M. Weathered, E. Kent, D. Kultgen, C. Grandy

Nuclear Sciences and Engineering Division
Argonne National Laboratory

October 2021

Contents

List of Figures

List of Tables

1 Executive Summary

The Flow Sensor Test Article (F-STAr) is a new test article under development for the Mechanism Engineering Test Loop (METL) which will provide high sodium flowrate capabilities for sensor, component testing, or fluid studies. Figure 1 shows two solid model renderings of F-STAr. The test article will include a high-capacity pump that can provide a nominal flowrate of 120 GPM; a versatile support structure which can accommodate a wide array of test sections, instrumentation, components, fluid studies, and more; and finally, a heating and cooling system to aid in controlling the testing environment. These main components are built off and mounted to standard ANSI flanges which aid in construction and assembly of the test article, giving experimenters flexibility in the design process to interchange components to fit their needs.

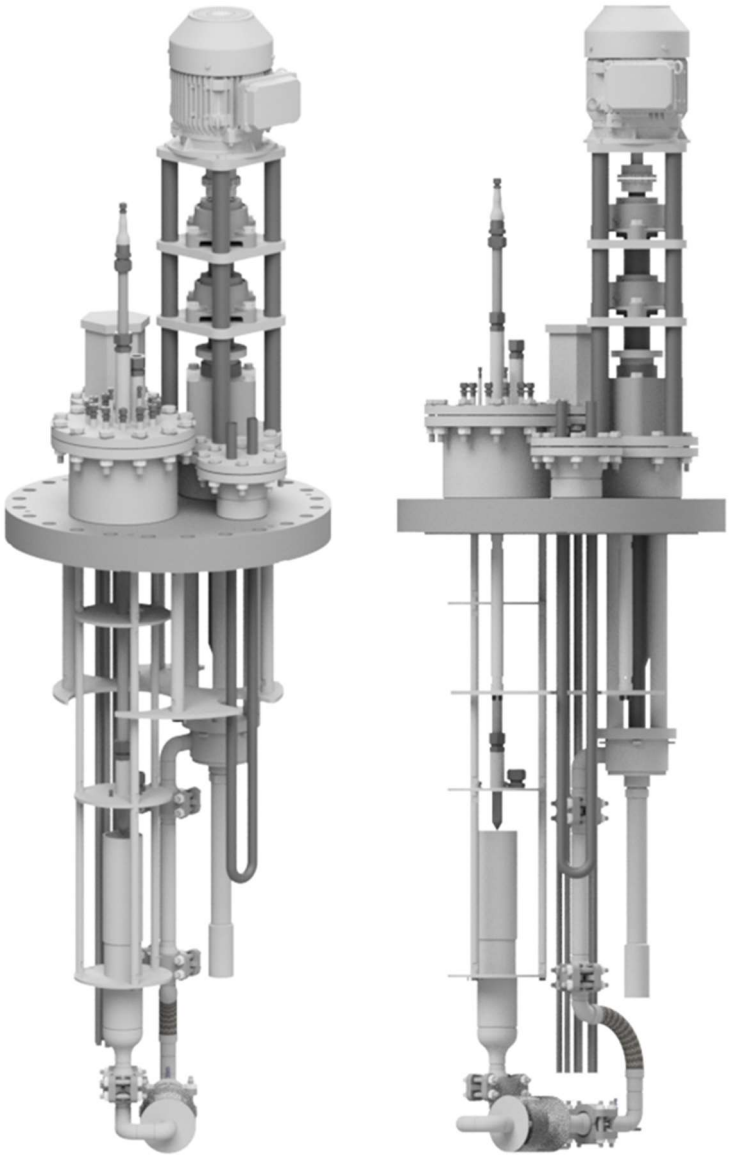

Figure 1 – A 3D rendering of F-STAr showing an isometric view (left) and an elevation view (right) with the Full-Scaled test section installed.

F-STAr's first deployment will be focused on developing and testing Sodium Fast Reactor (SFR) flow sensors located near the core fuel subassemblies outlet. The first type of flow sensor to be investigated will be Eddy Current Flow Sensors (ECFS) based on the RDT C4-7T standard. To accomplish this goal, the pump has been tailored to meet realistic nominal core assembly flowrates. Additionally, two test sections have been developed that model SFR outlet conditions; the "Full-Scaled" test section is designed to represent a single fuel handling socket; the "Pseudo-Scaled" test section is designed to represent a scaled array of fuel handling sockets. Figure 2 shows a pair of isometric views of both test sections. The dimensions of these two sections are based on socket dimensions found in literature of several SFR designs including the ABTR, AFR, ALMR, FASTER, and PRISM.

Although initially configured to study flow sensors, F-STAr can be configured to accommodate other experimental needs as well. For example, the test article could be outfitted with a test section that includes a scaled reactor fluidic diode or tests of hydrodynamic bearings. Other setups include fluid studies like thermal striping in the mixing area of two jets. Overall, F-STAr is designed to be a flexible facility which can provide high sodium flowrates for experimenters.

This report will review updates on the status of F-STAr. First, the report will describe a general overview of the test article and how each component interacts. Then, each main component will be discussed in a deep dive section which will review the design and other relevant details. F-STAr components which are discussed in more detail include the 120 GPM-pump, the support structure and test sections, 5 kW-heater, the 2 kW-cooler and cooling system, and the submersible flowmeter. Finally, this report will conclude with a brief recap and a bulleted outline of the path moving forward.

Figure 2 – Solid models of the Full-Scaled (left) and Pseudo-Scaled (right) test sections. These sections have been designed to represent a single handling socket and an array of scaled sockets, respectively.

2 Introduction

Several advanced power reactor designs are leveraging liquid metal's efficient energy carrying capabilities to improve plant safety and efficiency. Fluids such as liquid sodium have high heat transfer rates which improve heat removal from the reactor core relative to light water reactors. High heat transfer rates and large thermal powers in commercial reactor cores require large flowrates to achieve the desired core temperature rise. For example, many advanced nuclear plants have powers on the order of 500 MWth with a mean core temperature rise of 150 C which require total flowrates up to 50,000 GPM or higher [1] [2] [3] [4] [5] [6]. Divided into fuel subassemblies, the fluid velocities can be as high as 30 ft/s in some designs.

These high flowrates are important for reactor instrumentation where the signal output is scaled proportionally by the fluid velocity. One example includes advanced liquid metal flow sensors which are based on Lorentz Force principles. These sensors generate a signal which is linearly proportional the fluid velocity. However, testing these instruments at high flowrates can be challenging as it requires large capacity pumps and often large space requirements. Therefore, experimental capabilities for testing these instruments at more prototypic reactor core conditions is currently lacking.

To meet the needs for testing instrumentation and components at high flowrates, a METL vessel experiment call the Flow Sensor Test Article (F-STAr) has been designed. Figure 3 shows an annotated isometric view of F-STAr which identifies some of the main components. These components include a high-capacity pump capable of producing a nominal flowrate of 120 GPM; a flexible and versatile support structure which can accommodate a variety of test sections, instrumentation, components, fluid studies, and more; and lastly a heating and cooling system to achieve a variety of conditions required by the experimenter.

Each component in F-STAr is connected in an open loop which uses both the vessel and piping. Figure 4 presents a P&ID diagram showing the general flow path. First, the pump draws in fluid near the bottom of the vessel, discharging it into the test section piping. This piping is routed back to the bottom of the vessel and passes an open "drain port". Downstream from the drain is a submersible electromagnetic flowmeter. Finally, the fluid flows into a test section and is injected back into the vessel. Baffling near the sodium level reduces churning and protects the main vessel flange. The sodium then recirculates towards the bottom of the vessel and back to the pump inlet. Note that the P&ID omits the 5 kW heater and a 2 kW cooler and cooling system.

F-STAr's components are built and mounted on to standard ANSI flange patterns. This gives the experimenter flexibility during the design process to substitute components as needed. For example, a flowmeter setup could be exchanged with a fluidic diode, hydrodynamic bearing, or a fluid structure interaction test section, with the only requirement that these setups mount to the test section sub-flange and fit into the available opening. In another example, greater pumping capacity could be achieved by building the pump on the larger test section flange pattern. In F-STAr, individual components built on standard flange patterns form the building blocks to the test article and are interchangeable to meet the experimenter's needs.

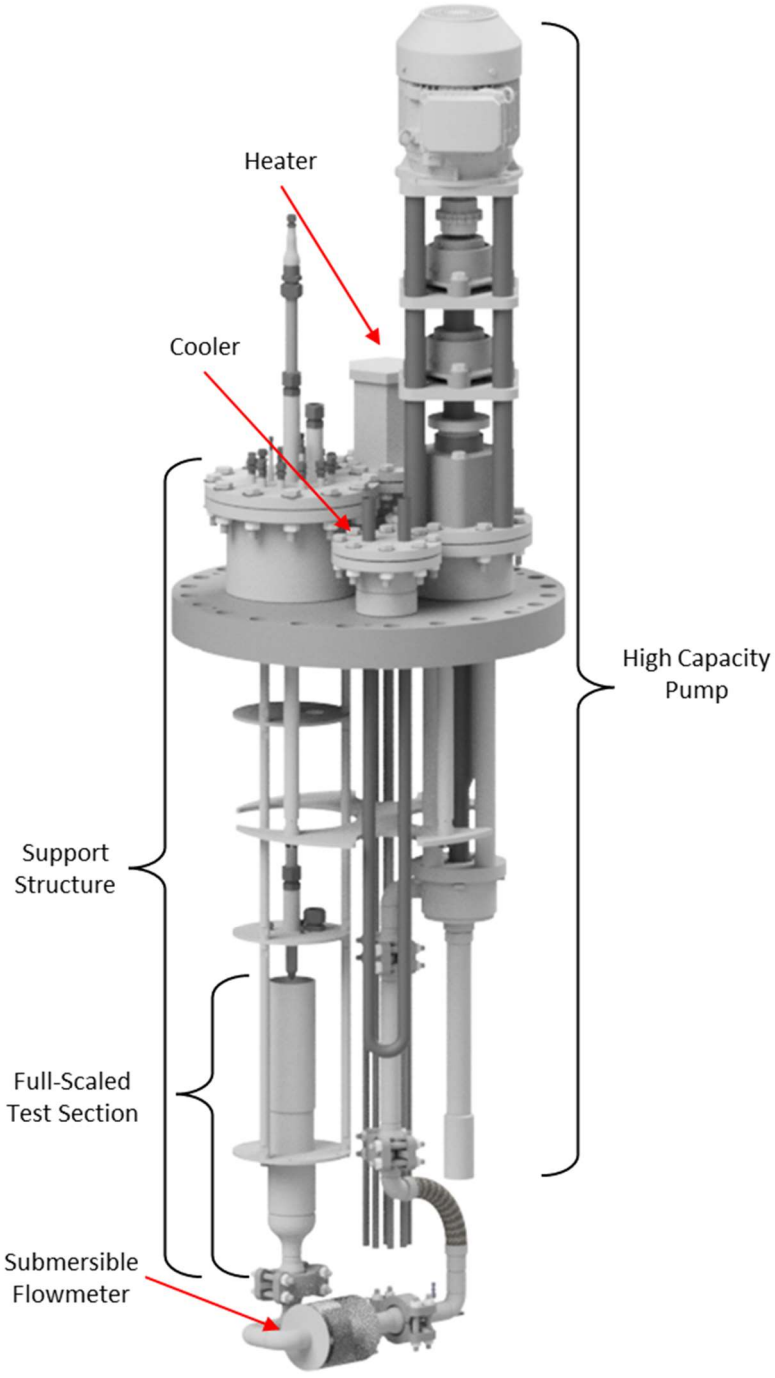

Figure 3 – An annotated isometric view of F-STAr showing the main test article components. Note that only the flange components are shown, and the 28-inch vessel is omitted.

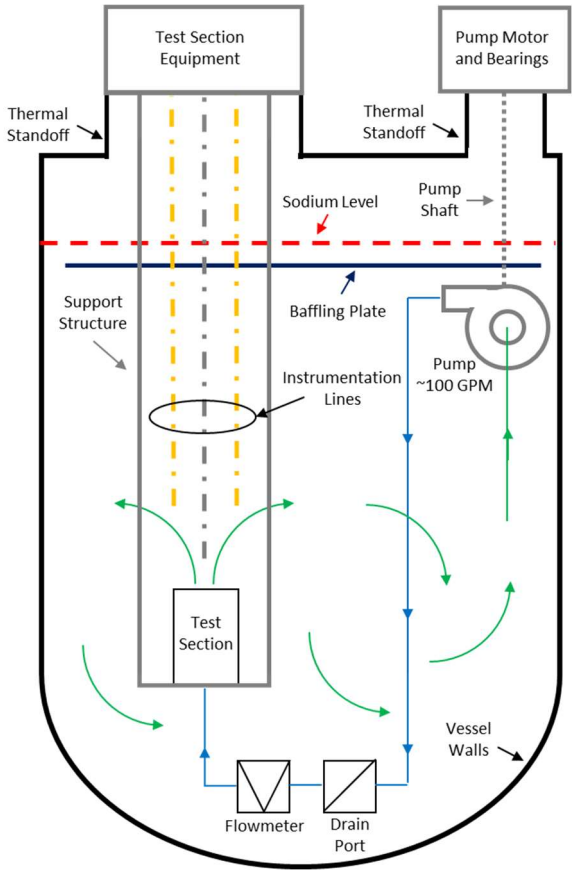

Figure 4 – Simple P&ID diagram of F-STAr.

Initially, F-STAr will be configured for developing and testing Sodium Fast Reactor (SFR) flow sensors, specifically Eddy Current Flow Sensors (ECFS). These sensors will be used to monitor the discharge flowrate from each subassembly in the SFR core. To accommodate this testing, F-STAr is equipped with a high-capacity pump which can provide realistic, single fuel subassembly flowrates. Additionally, two test sections are available which attempt to model the outlet SFR fuel subassembly. The first section represents a "Full-Scaled" fuel handling socket. The second section represents a "Pseudo-Scaled" array of fuel handling sockets.

During the flow sensor setup design, target flowrates and geometric conditions were identified in a literature review of several SFRs. These included the ABTR, AFR, ALMR, FASTER, and PRISM [1] [2] [3] [4] [5] [6]. Assembly flowrates were estimated by dividing the total reactor flowrate evenly between all core assembles. Additionally, fuel socket diameters, assembly pitches, and Upper Internal Structure (UIS) heights were identified. Since these characteristics varied between each design, their quantities were tabulated, and a nominal value was chosen to represent a generic SFR. Table 1 presents the design parameters used during the development of the flow sensor setup of F-STAr. Additionally, Table 1 presents the Pseudo-Scaled parameters and a hydraulic head estimate. These quantities and their derivation will be discussed in more detail later in the report.

Table 1 – Design parameters based on prototypical SFRs used during the development of F-STAr and the Full-Scaled and Pseudo-Scaled test sections.

Parameter	Units	Full-Scaled	Pseudo-Scaled
T	*F/C*	930/500	930/500
Assem. Flowrate	*GPM*	150	21
Required Head	*ft*	30-50	30-50
Socket Inner-Diameter	*in*	4	1.5
Socket Length	*in*	12	4
Socket Pitch	*in*	-	2.1
UIS Height	*in*	3	3

As mentioned earlier, while F-STAr will be initially setup for reactor core flow sensors, it can be easily reconfigured to perform a wide range of component testing and thermal hydraulic studies. For example, F-STAr's test section could be fitted to test a scaled fluidic diode. Figure 5 shows two elevation views of a hypothetical fluidic diode configuration: one in the "forward-flow" configuration the other in the "reverse-flow" configuration. Other possibilities include fitting a test section to study the performance of hydrodynamic bearings or to study thermal striping phenomena between adjacent fueling handling socket discharges. Overall, the test section can accommodate a variety of experimental needs.

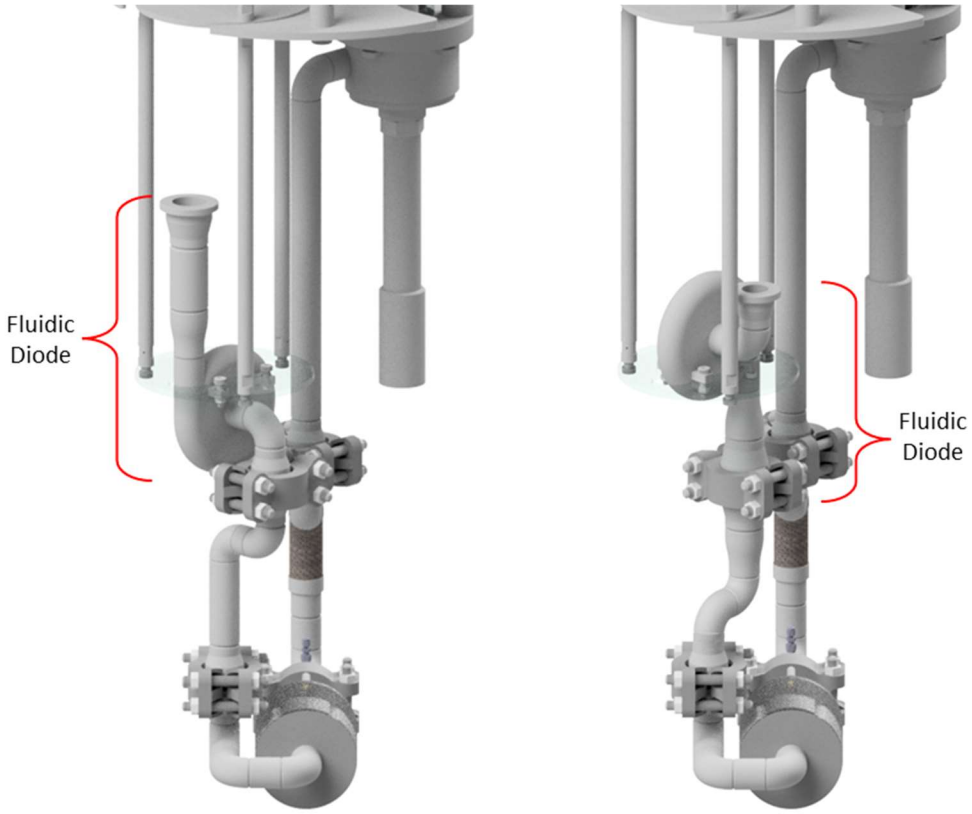

Figure 5 – Isometric view of a hypothetical fluidic diode configuration, installed in a forward-flow and reverse-flow configuration. F-STAr can also be fitted with a variety of other components for direct testing or sections for thermal hydraulic studies.

In summary, F-STAr will meet the needs of providing a versatile facility for large sodium flowrate testing capabilities. Since each F-STAr component is built on standard ANSI flanges patterns, the experimenter has flexibility during the design process to meet their individual requirements. Consequently, the test article can be outfitted with a variety of components such as a larger capacity pump, a fluidic diode, a hydrodynamic bearing, or setups for fluid studies such as fluid structure interaction studies. Initially, F-STAr will be configured to develop and test ECFS's near the outlet of a SFR fuel subassembly. As such, the pump and test section have been tailored to meet these needs. In total, F-STAr is designed to be versatile and capable of providing experimenters with a facility which can provide large flowrates for sensor, component, or thermal hydraulic studies.

3 Component Summary

F-STAr's initial configuration contains four major flange subcomponents. Figure 6 shows two isometric views of F-STAr annotated with these main components: the 120 GPM-pump, the support structure and test section, the 5 kW-heater, and the 2 kW-cooler and cooling system. Each of these components are built on standard 150 Class ANSI flanges which can then be installed on F-STAR's sub-flanges. Figure 7 shows an isometric view of the main flange with the welded sub-flanges.

Each building block component of F-STAr is lowered through an opening in its respective sub-flange and bolted in place. The heater and cooler sub-flanges are standard 5-inch 150 Class ANSI flanges which use standard reinforced graphite gaskets. Similarly, the pump and test section sub-flanges are patterned from 8-inch and 10-inch 150 Class ANSI flanges, respectively. However, in contrast to the heater and cooler, the pump and test section flanges are based on blind flanges and have a custom bore. This was done to maximize the opening size for these components. Consequently, these sub-flanges use custom energized C-ring seals in place of the standard graphite gasket seals. The C-ring seals seat in a groove located on the sealing face of the flange rather than a flat gasket face.

Another major F-STAr component denoted in Figure 6 is the submersible flowmeter. This sensor is a scaled-up copy of the submersible electromagnetic-type flowmeter designed for the Thermal Hydraulic Experimental Test Article (THETA) [7] [8]. The flowmeter will be used as a reference during the calibration and testing of ECFS's and other flow instrumentation. An advantage of these instruments is that they can be custom built and tuned to best measure the flowrates of a given experiment. Therefore, while the installed flowmeter is sized for ECFS testing, a new flowmeter can be designed and installed for any experiment which requires knowledge of sodium flowrates.

Overall, F-STAr's main flange supports the building block components and associated piping of the test article. Building and mounting components on to standard ANSI flange patterns provides the experimenter flexibility during the design process, allowing individual parts to be substituted or eliminated as needed. For example, a larger capacity pump could be installed on the test section sub-flange, while the pump sub-flange could be used to support a component study such a hydrodynamic bearing or fluidic diode or flow structure test section. In total, this method of mounting components to the main 28-inch flange provides significant versatility and flexibility.

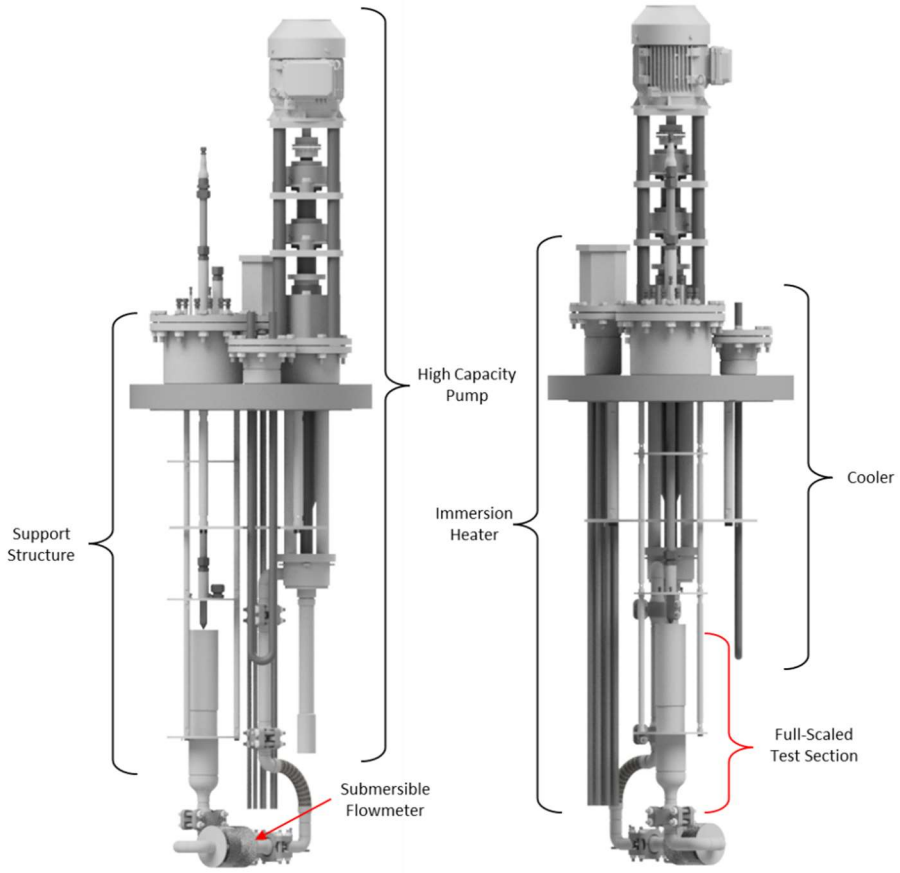

Figure 6 – Two elevation views of F-STAr configured with the Full-Scaled Test Assembly denoting the major components including the pump, test section, heater, cooler, and submersible flowmeter.

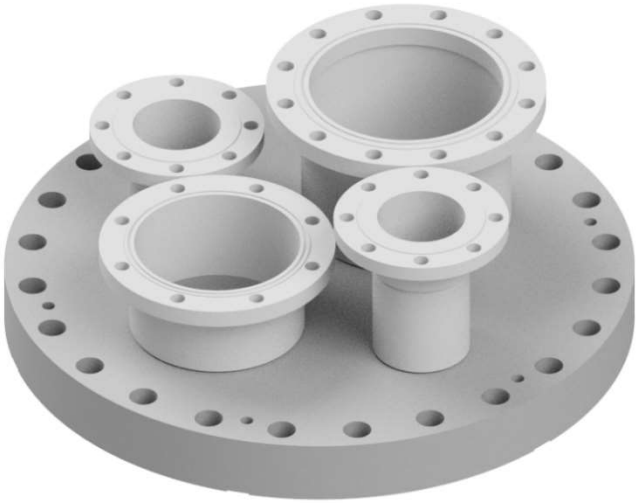

Figure 7 – F-STAr main flange and associated component sub-flanges.

3.1 Pump

3.1.1 Overview

F-STAr's pump is a custom high-temperature pump designed by an outside vendor. Figure 8 shows an isometric view and two elevation views of the as-designed pump. Table 2 presents an overview of the design specifications. The pump is built on an 8-inch 150-class ANSI blind flange which is mounted to a similarly patterned sub-flange on F-STAr's main flange. While most of the pump components can fit through the sub-flange opening, the volute casing must be removed and installed after mounting. In total, the pump is expected to deliver 100-120 GPM with a 5-inch impeller at a maximum speed of 3500 RPM. This is slightly below the desired target flowrate of 150 GPM. However, improvements to the delivery capacity could be made through an improved impeller casing seal design.

Figure 8 – Isometric and elevation views of the custom designed high-temperature pump.

Table 2 – Custom high temperature pump specifications.

Parameter	Value	Units
Temperature	1200/650	*C/F*
Nominal Flowrate	120	*GPM*
Impeller Diameter	5	*inches*
Immersion Depth	36	*inches*
Flange Mount	8-inch 150-class	
Motor	10/3500	*hp/RPM*

3.1.2 Estimated Pumping Capacity

A system head loss curve of F-STAr's plumbing was estimated using an equivalent lengths method. Figure 9 presents the estimated loss curve with the "Full-Scaled" test section installed. F-STAr's plumbing consists of 1.5-inch Sch40 piping, five short-radius elbows, four Grayloc hubs, and a 5-inch radius flexible bellows hose. Table 3 lists the absolute roughness values used on the piping and flow conditioner as well as the K-factors for the elbows and bellows hose. Some uncertainty exists in the K-factor for the bellows hose. Consequently, the estimated head losses were increased by a factor of 1.75 as a conservative estimate.

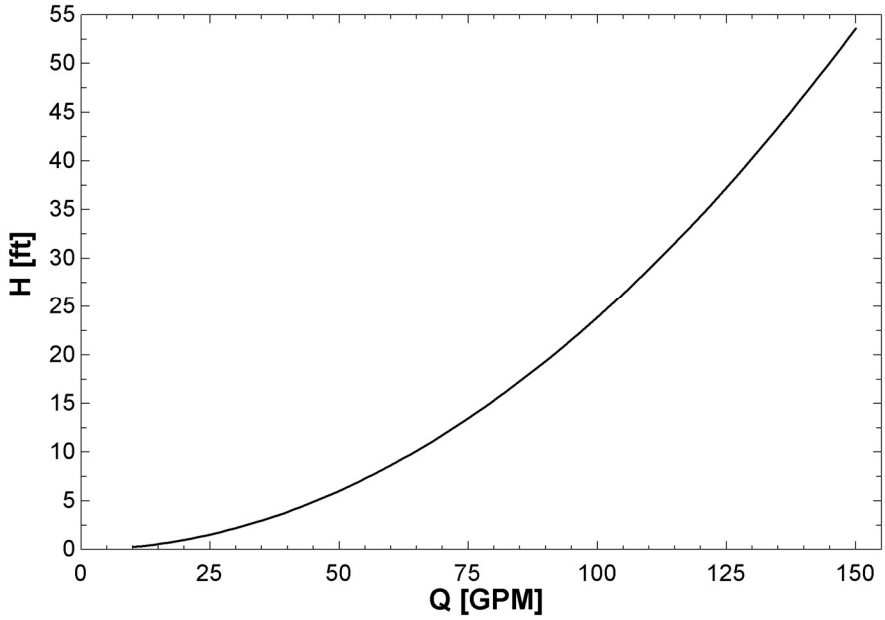

Figure 9 – Estimated head losses with the Full-Scaled Test Assembly at 250 C and a 1.75 safety factor.

Table 3 – Absolute roughness and K-factors used in the equivalent lengths analysis.

Parameter	Value	Units
Pipe Roughness	0.0015	*inches*
Flow Conditioner Roughness	0.0020	*mm*
Elbow K-Factor	0.28	-
Bellows K-Factor	0.60	-

3.1.3 Labyrinth Seal

The maximum pump flowrate delivery is expected to be roughly 100-120 GPM. This is below the desired design target of 150 GPM. To improve the maximum flowrate, a labyrinth seal is proposed to be installed between the shaft and the casing cover. Figure 10 shows an isometric view of the initial labyrinth seal design. The seal consists of a stack of fins which alternate between a wide and thin gap creating a tortuous flow path. This path is designed to increase the hydraulic resistance path along the shaft length. Consequently, this is designed to create a preferential flow direction towards the pump outlet versus the gap between the shaft and volute casing cover.

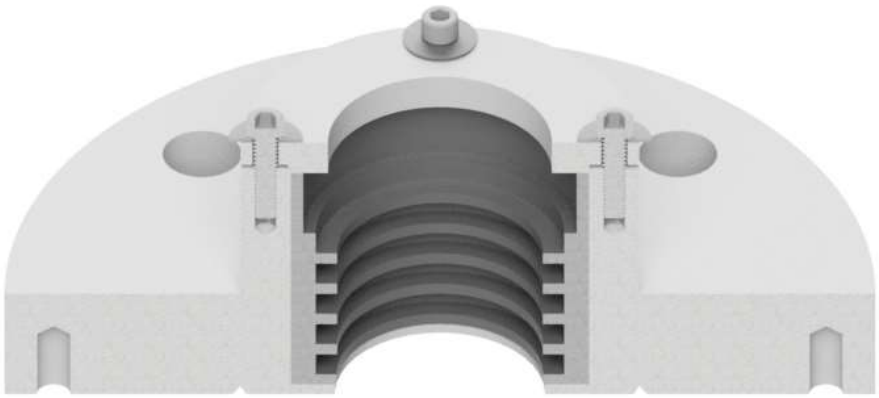

Figure 10 – Proposed labyrinth seal design mounted to the volute casing cover. The alternating narrow and wide gapped fins form a tortuous path for the flow along the shaft, increasing the hydraulic resistance.

Flow losses in the labyrinth seal were estimated using simple analytic theory [9]. Figure 11 shows the estimated labyrinth seal losses with the estimated system head losses. Note that factors of 1.5 were applied to decrease labyrinth head losses while a factor of 1.75 was applied to increase the system head losses. Due to uncertainties in these loss estimates, this figure crudely estimates a 20% leak rate through the seal. This estimate will be refined during water testing and may be an area of improvement if the pump still does not meet the desired performance.

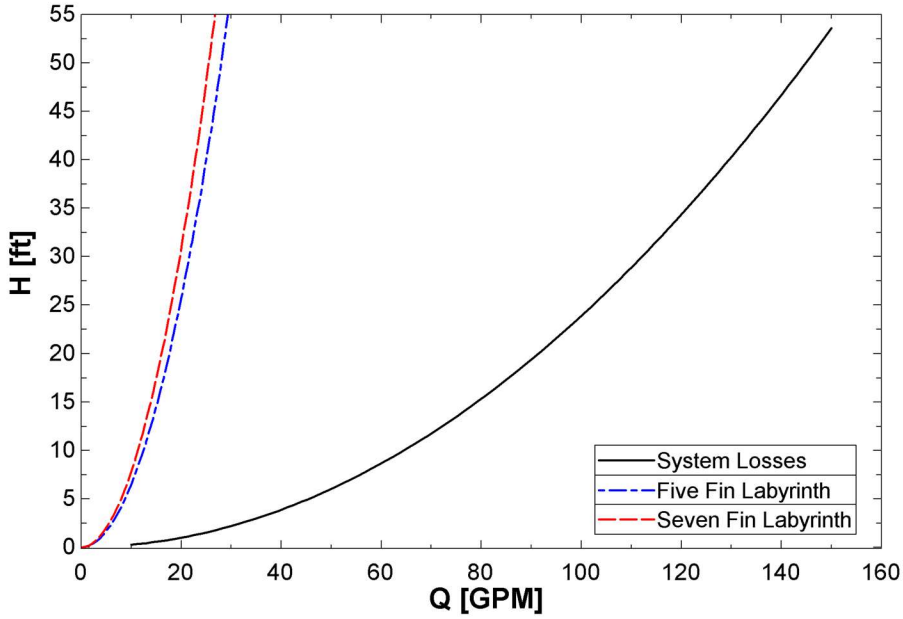

Figure 11 – Two labyrinth seal hydraulic loss curves with the estimated system losses. Note that the labyrinth seal losses were reduced by a factor of 1.5 while the system losses were increased by a factor of 1.75. Due to uncertainties in these calculations, this graph only provides a rough estimate of the leak rate at about 20%.

3.2 Support Structure

3.2.1 Overview

F-STAr includes a support structure used to suspend test sections and component subassemblies in the vessel. For its first deployment, F-STAr will test two models of reactor fuel subassembly handling sockets. Figure 12 shows an isometric view of the main structure and its sub-components which include the base-plate, UIS-plate, baffle-plate, support-ring, and support-struts.

The support structure is built off a standard 10-inch 150-class ANSI blind flange. Using a smaller blind flange avoids the complexity and expense of creating a new 28-inch vessel flange for each specific experiment. In this method, an experimenter can create any design and only needs to ensure that it avoids overloading a standard 10-inch 150-class blind flange, that the suspended structure fits through the specified opening, and that the structure avoids exceeding the maximum vessel depth.

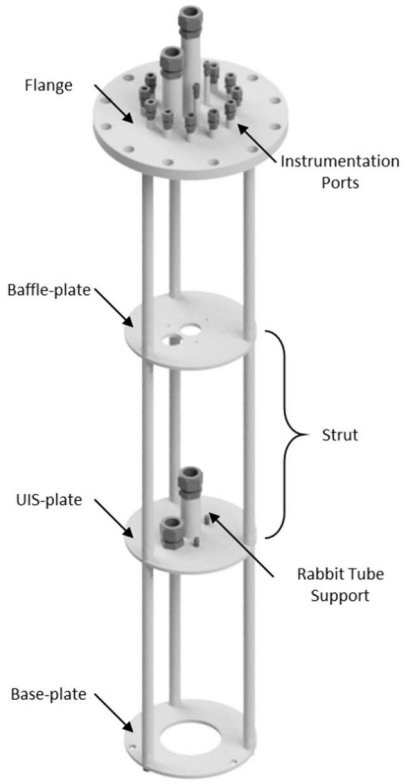

Figure 12 – Overview of the support structure designed to suspend the reactor fuel subassembly handling sockets models.

Figure 13 shows two isometric views of the support structure flange. The top-down view on the left shows the instrumentation ports. These ports are Swagelok compression fittings mounted to thermal stand-offs and will accommodate F-STAr's instrumentation such as thermocouples, signal wires, level sensors, and more. The bottom-up view on the right shows the support ring mounted to the flange. This support ring holds the load bearing struts which are used to support the base-plate and any test section assemblies.

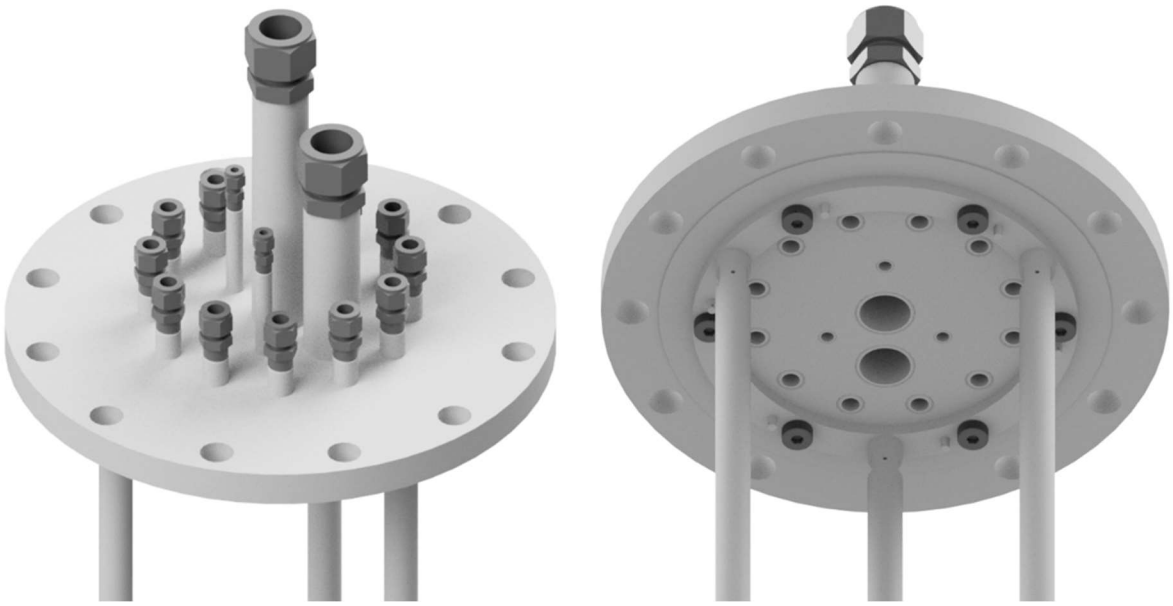

Figure 13 –Isometric detail view of the support structure flange. On the left is a top-down view of the flange showing the instrumentation ports. On the right is a bottom-up view of the flange showing the support ring which holds the load bearing struts.

Figure 14 shows a detailed isometric view of the UIS-plate. This sub-component is designed to simulate a solid UIS above a reactor core. The sizing of this plate is such that it encompasses the entire mean-jet diameter for the Full-Scaled test section or the outer most mean-jet diameter for the Pseudo-Scaled test section. Moreover, the UIS plate also supports three thermocouples and up to two rabbit tubes. These are supported by using Swagelok compression fittings.

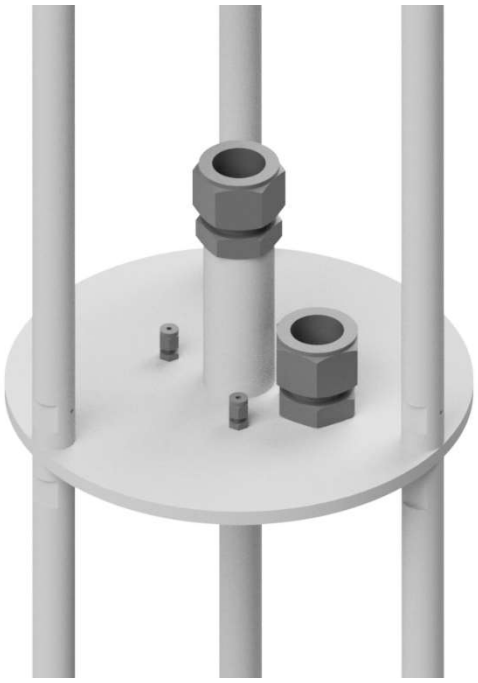

Figure 14 – Detailed isometric view of the UIS-plate.

3.2.2 Assembly Stand

One feature of F-STAr are the standardized flanges used to mount sub-components such as the cooler, heater, pump, and test section assemblies. This allows alternate sub-components to be built separately from the main flange. To aid in the assembly of the test section and support structure, a "Test Section Assembly Stand" has been designed. Figure 15 shows an isometric view of the assembly stand with a fully assembled test section. The assembly procedure begins by mounting the test section baseplate to the assembly stand vertical supports. Assembly proceeds by vertically stacking each sub-component until the support structure and test section subassembly are completed. Once assembled, the test section can be secured to a crane and mounted to F-STAr's sub-flange.

Figure 15 – Isometric view of the test section mounted to its assembly stand. Test section assembly begins by mounting the baseplate to the vertical support struts. Then the test section is assembled vertically from the baseplate, layering on each component above.

3.2.3 Bolt-Joint Analysis

The support structure uses bolted connections and vertical struts to support several suspended loads. Figure 16 shows a view of F-STAr looking up which denotes a few significant support structure loads. These loads include the test section assembly, Grayloc connection hubs, piping, flowmeter, and the balance of the support structure itself. Additionally, note that the flowmeter is cantilevered from the test section which will induce greater forces in support members due to the applied moment. Table 4 presents an estimate of the masses of each component which were used to estimate the loads on the bolted connections.

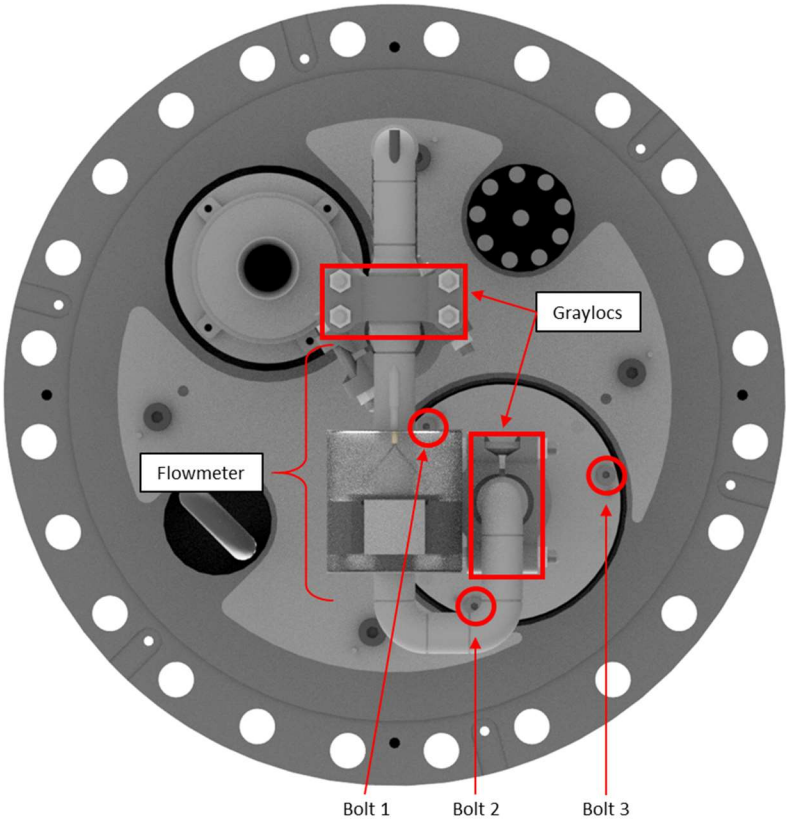

Figure 16 – Bottom-up view of the F-STAr flange showing some the high-mass components such as the Graylocs and Flowmeter, as well as the location of the support structure bolts. Note that the flowmeter and Graylocs are cantilevered.

Table 4 – Estimated masses of the test section sub-components.

Sub-component	Mass [lbm]
Flowmeter	26
Grayloc Hub-Ring-Clamp	15
Full-Scaled Test Section	45
Pseudo-Scaled Test Section	75
Balance	65

In addition to the sub-component masses and moments, the support structure will also experience live loads caused by fluid momentum. These momentum-induced loads were calculated and found to be mostly negligible. However, the fluid momentum entering and exiting the Full-Scaled test section was estimated to be 12 lbf at 200 C and 150 GPM. This load was added to the total sub-component mass and moment load. Table 5 presents the estimated maximum design load on any member of the test section structure.

This estimated design load was used to calculate a factor of safety (FOS). The absolute maximum load was calculated by using an estimated load bearing area and the 0.2% offset yield strength of 316SS at 550 C. Three analyses were completed. The first assumed the yield would occur at the bolt shank. Therefore, the load bearing area was assumed to be the shank itself. The second and third analysis assumed the yield would occur in either the internal or external threading. This is called the “pull out force” and estimates the maximum thread loading. The load bearing area was calculated using equations which estimated the thread shear area. Table 5 presents the calculated FOS for each case. These results suggest that the internal

threading has the lowest FOS. However, the minimum FOS is 47 times larger than the largest design load at the maximum temperature. Therefore, the threaded connections used in the support structure are expected to support the required loads in the most extreme conditions.

Table 5 – Estimated maximum design load applied to each strut and the Factor of Safety (FOS) for each support structure bolt in three cases: the shank case assumes the bolt shank yields, the Pull Out Internal assumes the internal threading yields, Pull Out External assumes the external threading yields. These FOS's were calculated using the 0.2% offset yield strength of 316SS at 550 C which is 25,000 psi.

Bolt	Max Design Load [lbf]	FOS		
		Shank	Pull Out Internal	Pull Out External
1	50	105	98	207
2	85	58	54	115
3	100	50	47	99

3.3 Full-Scaled Test Section

A model "Full-Scaled" SFR fuel handling socket was designed to simulate flow exiting a single sub-assembly for the study flow sensors in a single-jet configuration. Figure 17 shows a detailed view of the Full-Scaled test section which includes a Grayloc connector, inlet header, flow conditioner, and a modeled fuel handling socket, all mounted to a base-plate. The flow conditioner is used to help aid in developing the flow before entering the handling socket. Table 1 and Figure 17 denote some relevant dimensions of the test section. These dimensions are nominal and were chosen to capture the essence of a general full-scaled handling socket. In this setup, flow sensors such as ECFS's can be positioned in the socket centerline or 2.1-inches off the centerline path using the two available 1.25-inch instrument ports.

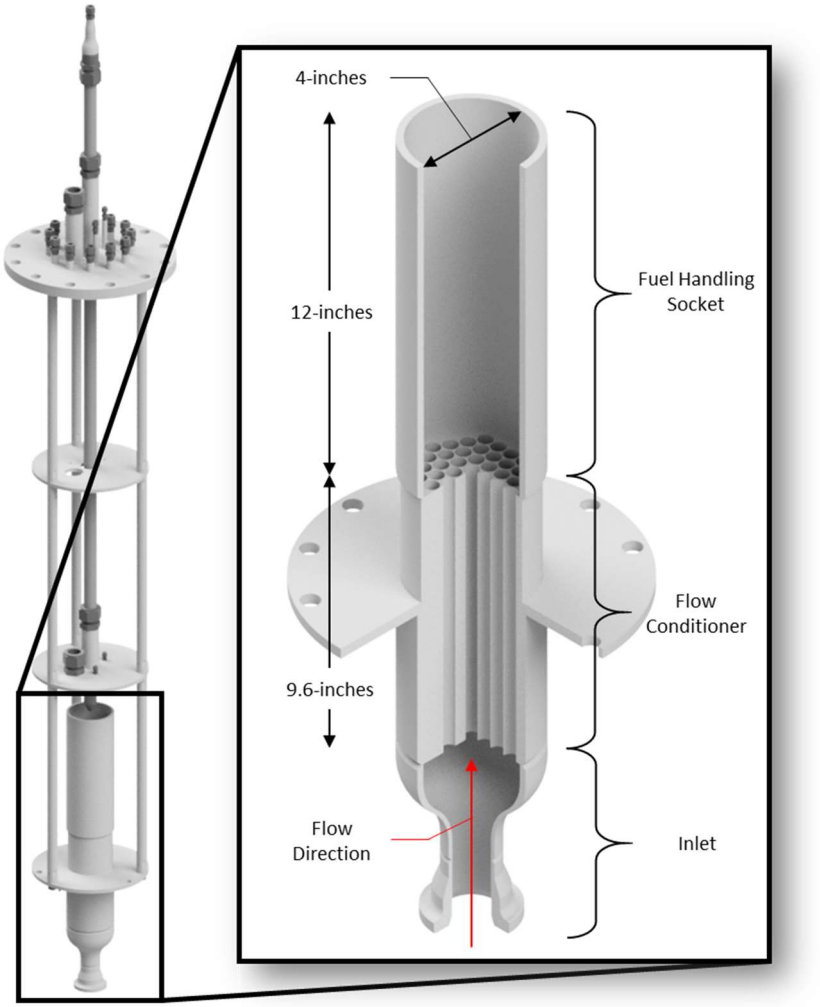

Figure 17 – Detailed isometric view of the Full-Scaled Test Assembly which includes a Grayloc connector, inlet header, flow condition, fuel handling socket, and base-plate. Dimensions of the socket denoted here and listed in Table 1 are nominal and were chosen to capture the essence of a prototypical SFR fuel handling socket.

3.4 Pseudo-Scaled Test Section

A model "Pseudo-Scaled" SFR fuel handling socket array was designed to simulate flow exiting an array of fuel sub-assemblies for the study flow sensors in a multi-jet configuration. This array was scaled due to vessel space constraints. The developed scaling approach in the test section design departs from the traditional approach of matching key non-dimensional numbers. Rather, this scaling methodology preserves the fluid velocity. Consequently, this approach is called "Pseudo-Scaling" to differentiate it from a true scaling mythology which matches non-dimensional numbers. Figure 18 shows a detailed view of the Pseudo-Scaled test section which includes an array of seven sockets. Each socket subassembly contains a flow conditioner and a scaled fuel handling socket. These subassemblies are welded to a base-plate which is also welded to an inlet header. At the inlet of the test section is a Grayloc hub which is used to connect to F-STAr plumbing. Table 1 and Figure 18 denote some relevant dimensions of the test section. In this setup, flow sensors can be positioned in the central socket centerline or in the centerline of the adjacent socket using the two available 1.25-inch instrument ports.

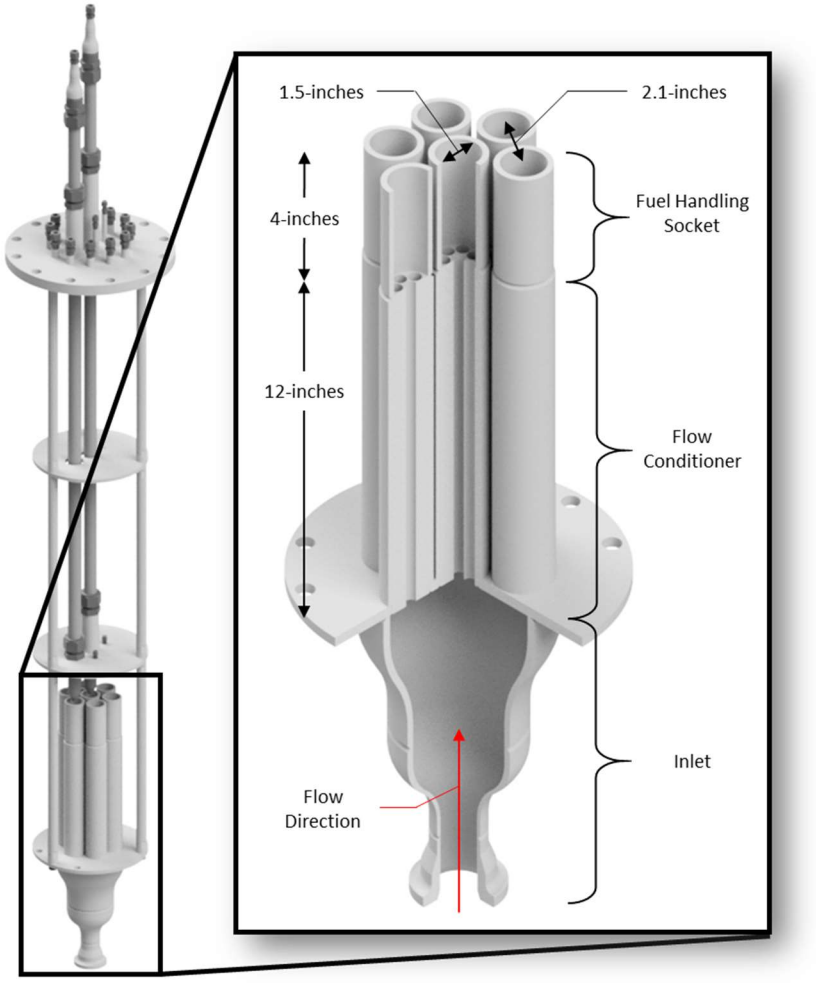

Figure 18 – Detailed isometric view of the Full-Scaled Test Section which includes a Grayloc connector, inlet header, flow condition, fuel handling socket, and base-plate. Dimensions of the sockets denoted here and listed in Table 1 were calculated from a "Pseudo-Scaling" analysis which preserves the exit velocity.

3.4.1 Pseudo Scaling Methodology

In this work, the scaling methodology departs from a true scaling analysis which aims to match characteristic non-dimensional numbers. Rather, the scaling approach in this work aims to match the socket outlet velocity. While non-traditional, this methodology was justified by noting the functional dependence of permanent-magnet and field-shift based flowmeters on the fluid velocity. Consequently, this scaling methodology is called "pseudo-scaling" to respect that it departs from a true scaling analysis. Table 1 presents the results from the scaling analysis in the "Pseudo-Scaled" column.

To start the pseudo scaling analysis, the scaled socket diameter was found by directly matching the prototypical "Full-Scaled" (FS) and "Pseudo-Scaled" (PS) mean socket velocity. Equation 1 calculates the pseudo-scaled socket diameter D_{ps} from the full-scaled socket diameter D_{fs}, the number of scaled sockets n_s, the expected nominal pump flowrate Q_{pump}, and the average full-scaled socket flowrate Q_{fs}. Note that Q_{fs} is a nominal value taken from dividing the total core flowrate through all subassemblies. Figure 19 plots Equation 1 as a function of Q_{pump}/Q_{fs}.

$$D_{ps} = D_{fs} \cdot \sqrt{\frac{1}{n_s} \cdot \frac{Q_{pump}}{Q_{fs}}}$$

Equation 1

After scaling the socket diameter, the UIS height was scaled. This was done by matching the velocities of the full-scaled centerline jet impinging on the UIS to a single pseudo-scaled socket jet impinging on the model UIS. Equation 2 was used to calculate the centerline velocity U_{CL} from the socket velocity U_s, socket diameter D_s, and the UIS height H_{UIS}. By matching the full-scaled and pseudo-scaled socket velocities and solving for the ratio of pseudo-scaled to full-scaled UIS height, Equation 3 was derived. Note that Equation 3 and Equation 1 are the same function. Therefore, the ratio of pseudo-scaled to full-scaled socket diameter and UIS height is simply denoted as $L_{scaled}/L_{full-scale}$ in Figure 19.

$$\frac{U_{CL}}{U_s} = 6 \cdot \frac{D_s}{H_{UIS}}$$

Equation 2

$$\frac{H_{UIS,ps}}{H_{UIS,fs}} = \sqrt{\frac{1}{n_s} \cdot \frac{Q_{pump}}{Q_{fs}}} = \frac{L_{scaled}}{L_{full-scale}}$$

Equation 3

Finally, the pseudo-scaled UIS diameter was chosen such that it encompasses the outer most nominal jet diameters. Equation 4 was used to calculate the nominal jet diameter D_{jet} from the UIS height. Figure 20 plots ratio of jet diameter to UIS height as a function of $L_{scaled}/L_{full-scale}$. Note that the jet diameter to UIS height ratio is constant for any value of D_{ps}/D_{fs} or $H_{UIS,ps}/H_{UIS,fs}$.

$$D_{jet} = 4 \cdot (0.09\ H_{UIS})$$

Equation 4

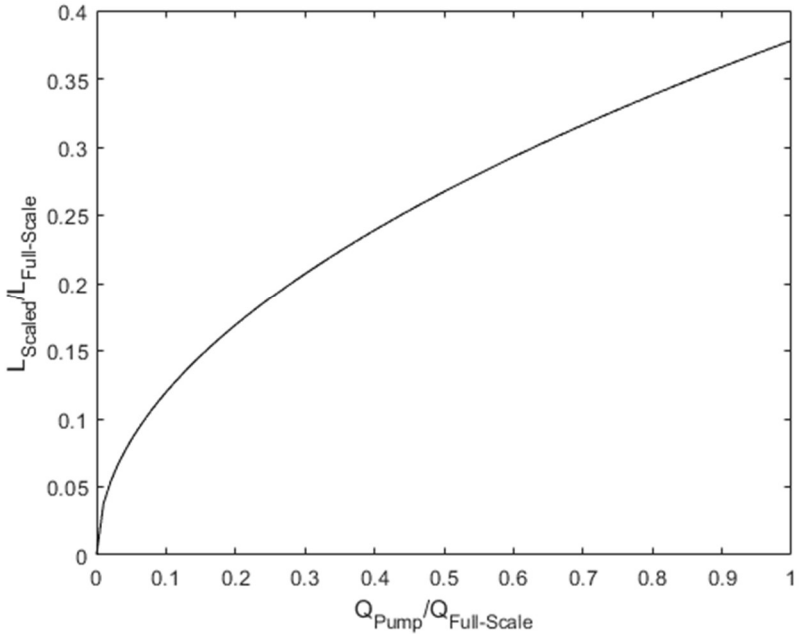

Figure 19 – Equation 1 plotted as a function of nominal pump flowrate to the nominal averaged socket discharge flowrate. Note that the pseudo-scaled to full-scaled socket diameter ratio is the same function as the UIS height ratio. Therefore, these ratios are simply denoted as $L_{scaled}/L_{full-scaled}$.

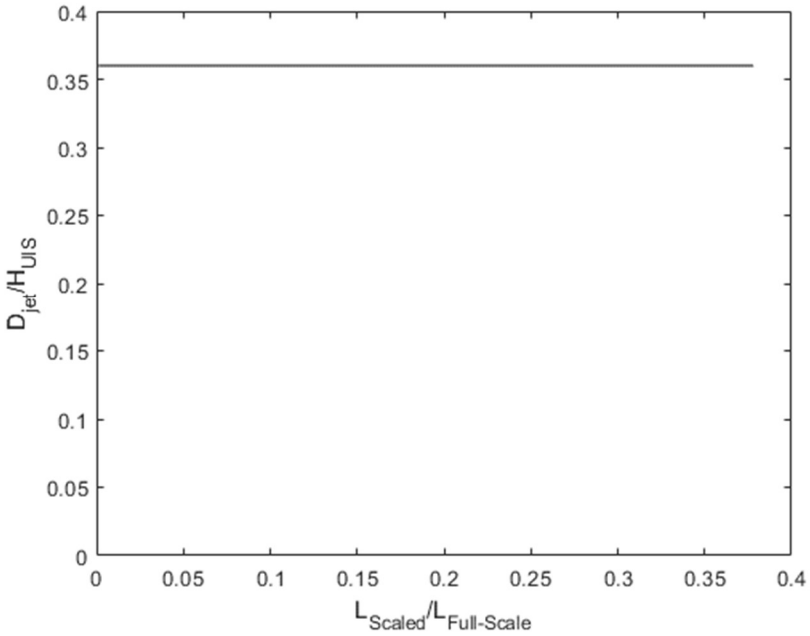

Figure 20 – Equation 4 plotted as a function of $L_{scaled}/L_{full-scaled}$. *Note that the jet diameter to UIS height ratio is constant for any value of* D_{ps}/D_{fs} *or* $H_{UIS,ps}/H_{UIS,fs}$.

3.5 Immersion Heater

3.5.1 Overview

Heating of F-STAr is supplemented by a custom immersion heater designed and constructed by an outside vendor. The heater is designed to avoid direct contact of heating elements with the fluid by inserting them into a protective sheath. An advantage of this design is that individual heating elements can be replaced without removing the whole unit from the sub-flange, reducing downtime in the event of a heating element failure. This is accomplished by inserting the heating elements into a sealed sheath which is in direct contact with the fluid. Figure 21 shows an overview of F-STAr's heater while Table 6 outlines some system specifications. Several specifications are listed in the "other" category which are concerned with the quality assurance of the sheath tube welds due to the sheaths being a primary containment barrier.

Figure 21 – Isometric view of the custom designed and built heater.

Table 6 – Outline of immersion heater specifications. "Other" specifications are concerned with the quality assurance of the sheath tube welds.

Specification	Value	Unit
Power	5	*kW*
Immersion Length	72	*inch*
Cold Length	43	*inch*
Elements	9	-
Electrical	• 480VAC, 3ph, 6 amp	
Mounting Flange	• 5", 150#, 316/316L	
Sheathing	• Incoloy 800, seamless	
OT Protection	• Type K TC on sheath	
Other	• MTRs on wetted components. • Hydrostatic test at 71 F and 70 psig. • Dye penetration test on wetted welded components.	

3.5.2 Estimated Heating Requirements

Dry heat-up tests of Vessel 3 revealed that thermal leakages were significant. These tests were halted prior to achieving 650 C due to the temperature of Zone 2 lagging by more than 50 C. Consequently, additional heating capacity is desired to aid in offsetting thermal leakages and temperature control.

The additional power required by Zone 2 was estimated by using a simple thermal resistance analysis. Equation 5 was used to define an average thermal resistance for a particular heat zone using recorded test data. These data included the equilibrium temperature T_{SS} and associated PID percentage. Table 7 presents the installed power for each vessel zone, the estimated thermal resistances, and finally the duty cycles required for each zone to reach T_{SS} of 650 C. One can see that Zone 2 requires approximately 33% more power than installed or roughly 1 kW.

$$R\left[\frac{C}{W}\right] = \frac{T_{SS}[C] - T_0[C]}{Duty \cdot P_{max}\,[W]}$$

Equation 5

Table 7 – Estimated thermal resistances "R" and required duty cycle to achieve 650 C with an empty vessel. Note that Zone 2 will require roughly 33% more power, or about 1 kW.

Zone	P [kW]	R [C/W]	Duty(T_{SS} = 650 C) [%]
1	2.4	1.39	18.8%
2	3.0	0.16	132%
3	5.3	0.12	95.0%
4	3.6	0.21	81.3%

There are a few caveats to the power leakage analysis. Firstly, the ambient air temperature was left unreported, and the convection coefficient may not have been constant during testing. This will impact the magnitude of the calculated thermal resistance. Secondly, only a single data point was measured and is being used over the total range of operating temperatures. However, the thermal resistances may vary with temperature due to thermal conduction effects between zones or other factors. Therefore, this analysis should be used with caution.

The next step in the analysis was estimating the required power to heat up the sodium from an assumed fill temperature of 250 C to 600 C. In this analysis, the heat rate is limited to 0.02 C/min to prevent over-stressing the vessel. Equation 6 was used to estimate the heater power where $\rho(T_{op})$ is the density of sodium at operating temperature, V_{vessel} is the vessel volume, $c_p(T_{avg})$ is the specific heat capacity of sodium at operating temperature, and τ is the heat-up rate. Note that the sodium volume is constant due to the overflow port on the vessel. Consequently, the mass of sodium will decrease with increasing temperature resulting in less heater power.

$$P_{Na,T_{op}}[W] = \rho(T_{op})[kg/m^3] \cdot V_{vessel}[m^3] \cdot c_p(T_{avg})\left[\frac{J}{kg} \cdot C\right] \cdot \tau[C/s]$$

Equation 6

Figure 22 shows the results of the analysis which also included power losses from component thermal stand-offs, and parasitic power losses in addition to the required power to heat the sodium volume at 0.02 C/min. Note that when the vessel heater power is aggregated, there is sufficient power to balance the parasitic heat losses. This is not true when the vessel is empty. However, the addition of sodium in the vessel may promote conduction from Zone 1 and Zone 3 which may counteract the lagging the Zone 2. Nevertheless, F-STAr's heater was specified with 5 kW of power to aid in the vessel heating and temperature control.

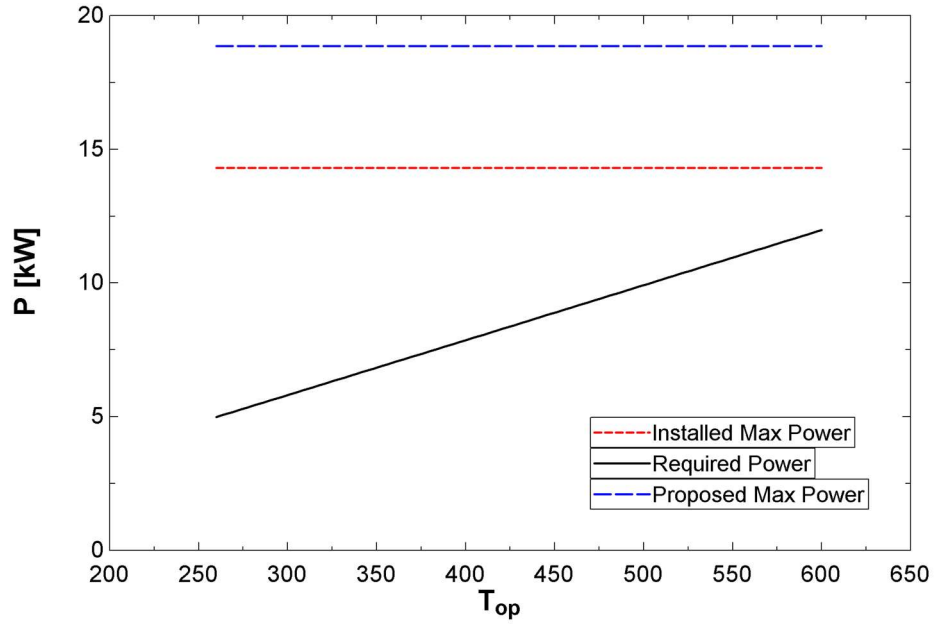

Figure 22 – Estimated power requirements to heat the vessel and sodium to Top at a rate of 0.02 C/min. This analysis includes the vessel and proposed thermal stand-off leakages as well as the power required to heat the sodium.

3.6 Cooler

3.6.1 Overview

A cooler was designed to aid in steady-state testing by removing heat input from the pump and frictional losses. Figure 23 shows an isometric view of the cooler. In principle, the cooler uses an inert gas flowing through a 1.25-inch thin-wall tube with a single uniform 3.25-inch bend at the bottom. This tube bend is welded to the bottom to a standard 5-inch 150-class blind ANSI flange. Connections to a cooling system are made at top via Swagelok fittings. By using argon gas and a sodium temperature of 250 C, this cooler can remove approximately 2 kW of thermal power at a flowrate of 25 CFM.

Figure 23 – Isometric view of the cooler installed on F-STAr's main flange.

3.6.2 Estimated Cooling Requirements

Heat input from the pump and frictional losses will be a significant problem at high flowrates and low operating temperatures. Assuming a 10 hp pump with an efficiency of 25%, the heat input is estimated to be roughly 5.5 kW. This power can be removed by leveraging the vessel parasitic losses. However, these losses will be insufficient at low temperatures. Figure 24 presents the estimated vessel losses as a function of operating temperature. At the lowest operating temperature of 200 C, a cooler will need to remove roughly 2 kW of power to supplement the vessel losses.

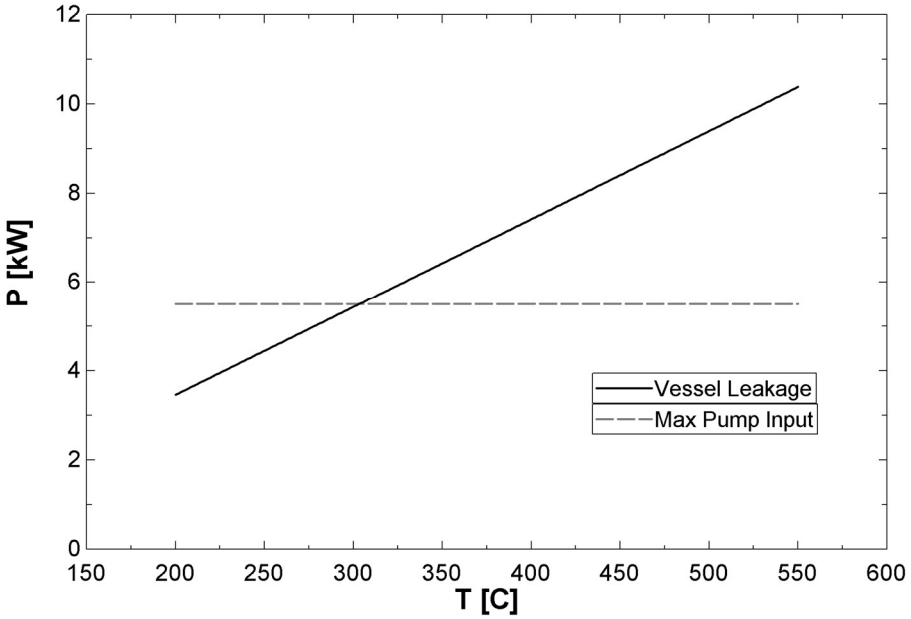

Figure 24 – Estimated vessel power leakage as a function of operating temperature. In grey is the estimated heat input from the pump. Between operating temperatures of 200 C and 300 C, a cooler will be needed to supplement the vessel losses.

A heat transfer and thermodynamic analysis were completed to estimate the cooler power removal rate and outlet temperature as a function of argon gas flowrate. Figure 25 shows that roughly 35 CFM of argon at an inlet temp of 20 C will remove approximately 2 kW of power from an isothermal pool of sodium at 200 C. The analysis was only completed for temperatures up to 300 C since it's estimated that the vessel parasitic heat losses will be able to remove the input power at higher temperatures. The final rejection of this power will be discussed in the cooling system section of the report.

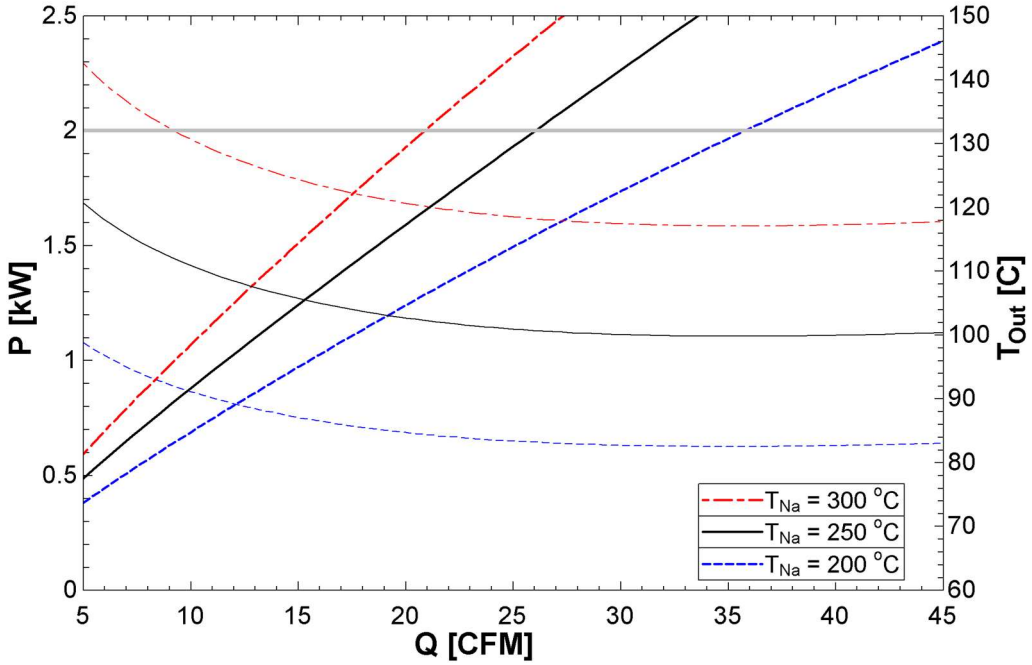

Figure 25 – Estimated cooler power removal and outlet temperature as a function of argon gas flowrate and sodium pool temperature for three sodium pool temperatures.

3.7 Argon Cooling System

3.7.1 Overview

In Section 3.6, a heat transfer analysis estimated that 5 kW of power could be removed via parasitic heat losses through the insulation down to an operating temperature of 300 C. However, between 200-300 C these heat losses will need to be supplemented by additional cooling. Thus, Section 3.6 also estimated the cooling power of a simple U-tube immersion cooler using argon gas. The heat transfer results showed that about 35 CFM of argon would be sufficient to remove about 2 kW of power at a sodium temperature of 200 C.

Delivering these flowrates and final rejection of the 2 kW of thermal power will be accomplished by a closed-circuit argon cooling loop, which is simply called the "cooling system". Figure 26 shows a P&ID of the cooling system which contains a blower, a heat exchanger, and a by-pass leg. The blower is a 5 hp regenerative blower capable of delivering 379 CFM of air at 7.94 psi, maximum. The heat exchanger is a 998,000 BTU/hr brazed-plate heat exchanger using city water as the ultimate heat sink. Finally, the by-pass leg and globe valve will aid in flow control.

Figure 27 shows an isometric of the cooling system connected to F-STAr's cooler while Figure 28 shows a detailed isometric view of just the loop. The cooler piping is 2-inch Sch 40 connected via Graylocs. Between the loop and F-STAr are flexible bellows hoses which will absorb any thermal expansion, dampen vibrations, and accommodate some misalignment.

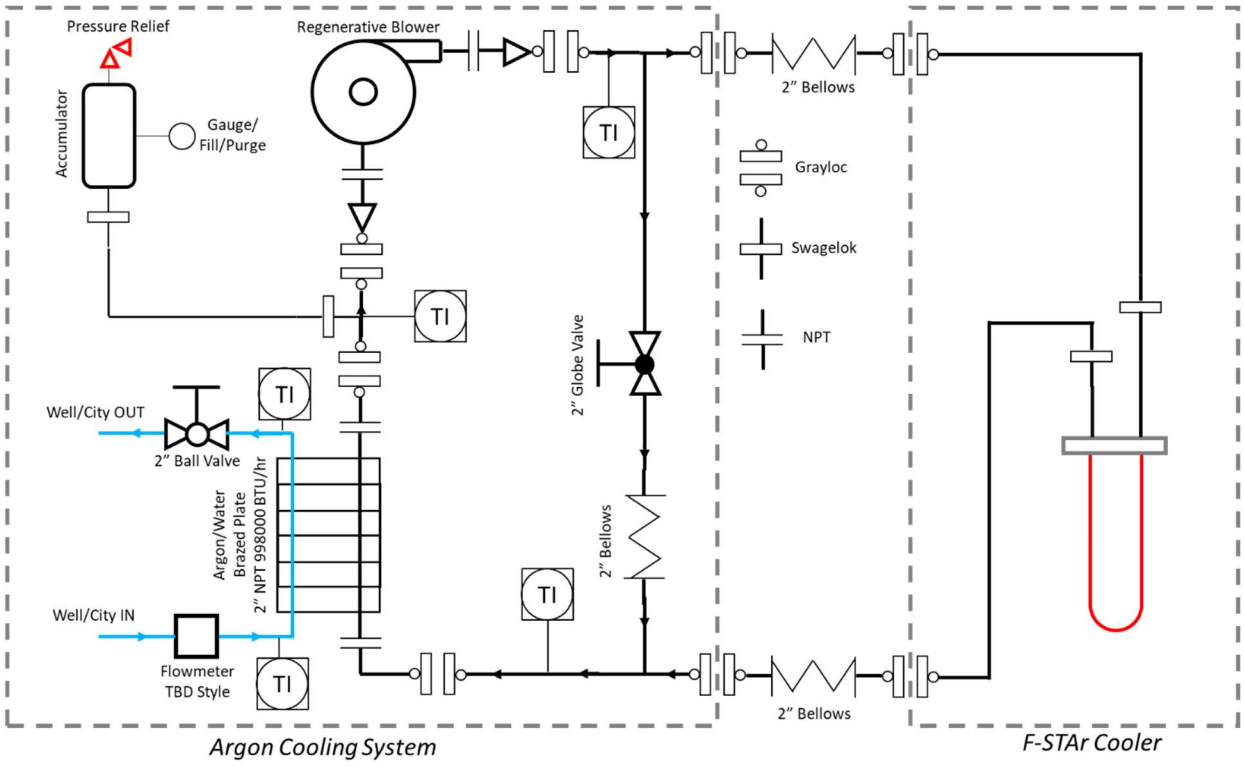

Figure 26 – P&ID of the cooling system and cooler. The cooling system consists of a stand-along rig plumbed into the F-STAr U-Tube cooler which is attached via flexible bellows hoses. The main cooling system consists of a 5 hp regenerative blower, a 998,000 BTU/hr brazed-plate heat exchanger as the ultimate heat sink, and a by-pass leg with globe valve, all plumbed with 2-inch Sch40 pipe and Graylocs.

Figure 27 – Isometric view of the argon cooling system connected to F-STAr's cooler. The loop and F-STAr are connected by flexible bellows hoses which will absorb any thermal expansion, dampen vibrations, and accommodate some misalignment.

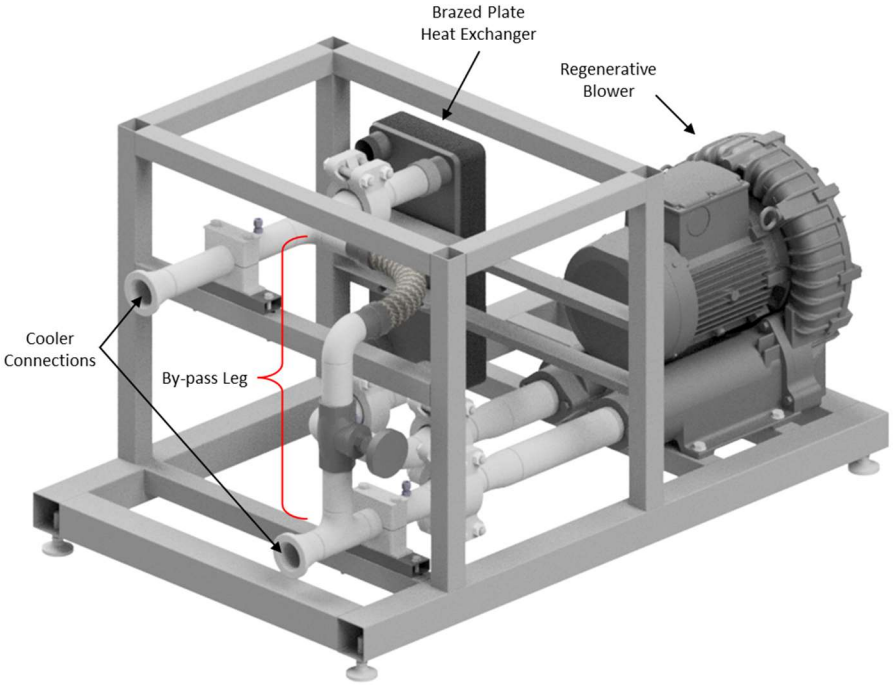

Figure 28 – Detailed isometric view of the argon cooling system. The loop piping is 2-inch Sc40 connected with Graylocs.

3.8 Submersible Flowmeter

3.8.1 Overview

For its first deployment, F-STAr is configured to develop, test, and calibrate reactor core outlet flow instrumentation such as ECFS's. Studying these sensors requires the accurate measurement of flowrates by a reference flowmeter. Satisfying this requirement is a high-temperature submersible Electromagnetic Flowmeter (EMFM). This flowmeter is a scaled-up version of the highly successful design by Matthew Weathered for use in THETA [7] [8]. Figure 29 presents an isometric view of F-STAr's EMFM which is designed to measure flowrates from 10 GPM to 100 GPM or higher with a maximum operating temperature of 550 C. The components shown in Figure 29 are hermetically sealed by a 6.25-inch diameter tube which is backfilled with argon gas. More details on the mechanical design of this flowmeter can be found in THETA's status report [7] [8].

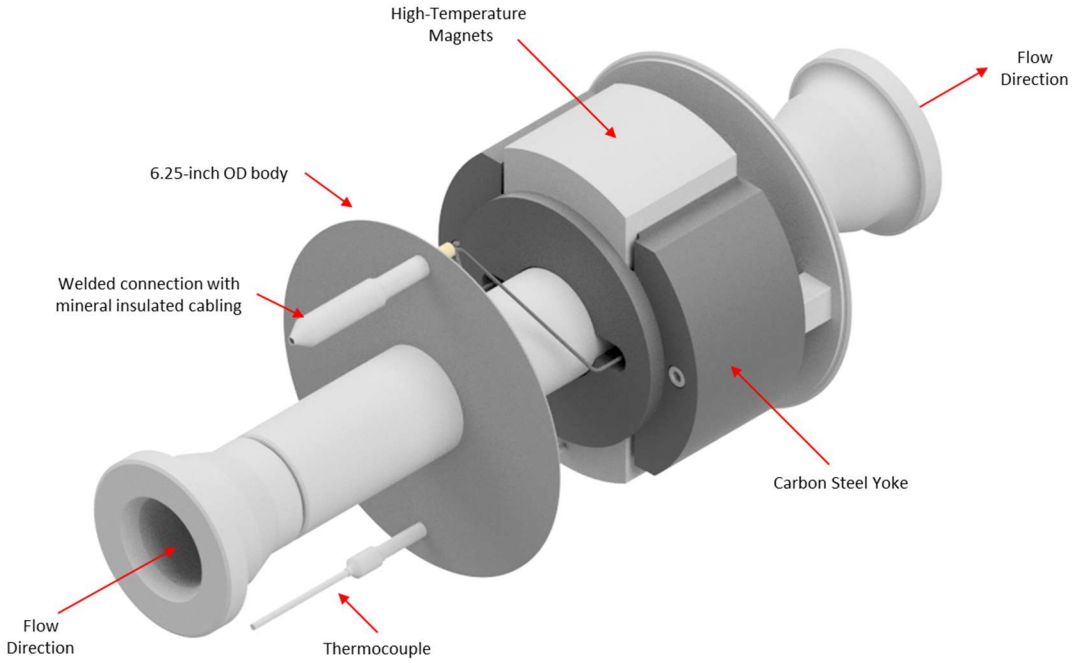

Figure 29 – Isometric of F-STAr's submersible EMFM. Note that the cover tube is invisible to aid in showing the internal components.

3.8.2 Estimated Signal Output

F-STAr's reference flowmeter components were sized using established EMFM theory. In principle, an EMFM correlates flowrate to the induced voltage produced by an electrically conductive fluid passing through a stationary magnetic field. Note that a magnetic field oriented perpendicular to the fluid velocity will induce a mutually orthogonal voltage that can be measured by a pair of externally mounted electrodes. These measured voltages ΔV_{EMFM} are related to volumetric flowrates Q velocity by Equation 7 where K_1, K_2, K_3 are correction factors, and B_0 is the magnetic field magnitude across the inner tube diameter d_i [10].

$$\Delta V_{EMFM} = K_1 K_2 K_3 B_0 \frac{4}{\pi} \frac{Q}{d_i}$$

Equation 7

Factor K_1 in Equation 7 corrects for wall-shunting effects. Equation 8 defines K_1 where d_i and D_o are the conduit inner and outer diameters respectively, while ρ_f and ρ_w are the fluid and conduit electrical resistivity respectively [11] [12] [13]. Note that the wall temperature is assumed to be the same as the sodium temperature.

$$K_1 = \frac{\frac{2d_i}{D_o}}{1 + \left(\frac{d_i}{D_o}\right)^2 + \frac{\rho_f(T_{Na})}{\rho_w(T_{Na})}\left(1 - \left(\frac{d_i}{D_o}\right)^2\right)}$$

Equation 8

Correction factor K_2 corrects for end-shunting at the inlet and outlet of the flowmeter where the magnetic field is weakest. Equation 9 defines the K_2 where L is the flowmeter length and d_i is the inner diameter of the conduit [14] [15] [16] [17]. Note that this form is only valid for $1 \leq \frac{L}{d_i} \leq 3.5$.

$$K_2 = -0.0047\left(\frac{L}{d_i}\right)^4 + 0.0647\left(\frac{L}{d_i}\right)^3 - 0.3342\left(\frac{L}{d_i}\right)^2 + 0.7729\left(\frac{L}{d_i}\right) + 0.3172$$

Equation 9

Lastly, correction factor K_3 corrects for magnet temperature effects. Equation 10 defines the K_3 where T_{mag} is the magnet temperature in °C [18]. The K_3 used in this work is the same used during the development of THETA's EMFM.

$$K_3 = 1.1646 \cdot \left(-7 \times 10^{-7} \cdot T_{mag} + -2 \times 10^{-4} \cdot T_{mag} + 0.8587\right)$$

Equation 10

Note that the theoretically induced voltage described by Equation 7 is directly proportional to the volumetric flowrate and magnetic field strength while inversely proportional to the inner diameter of the flowmeter. These parameters are important in F-STAr's EMFM which uses a larger conduit diameter than THETA's. Consequently, not only will increasing the conduit diameter reduce the voltage proportionally, but it will also increase the magnet spacing, which reduces the magnetic field strength, also decreasing the voltage proportionally. At large flowrates, this is of little concern. However, at low flowrates the signal becomes weak and noisy. Therefore, for F-STAr's EMFM to be accurate at low flowrates, a new magnet geometry was designed to increase the magnetic field strength.

Defining the geometry first started with a 2D finite element model that was constructed and evaluated using Finite Element Method Magnetics (FEMM). Figure 30 show the construction and contour plot of the resulting flux density. The magnets were mounted to a steel yoke which not only fixes them in place but also increases the magnetic field amplitude. From Figure 30, three vertical cuts were plotted. Figure 31 plots the centerline cut at 0-inches and ±0.3125-inches. These plots show that the magnetic field is relatively uniform across the flowmeter conduit with an average value of approximately 260 mT.

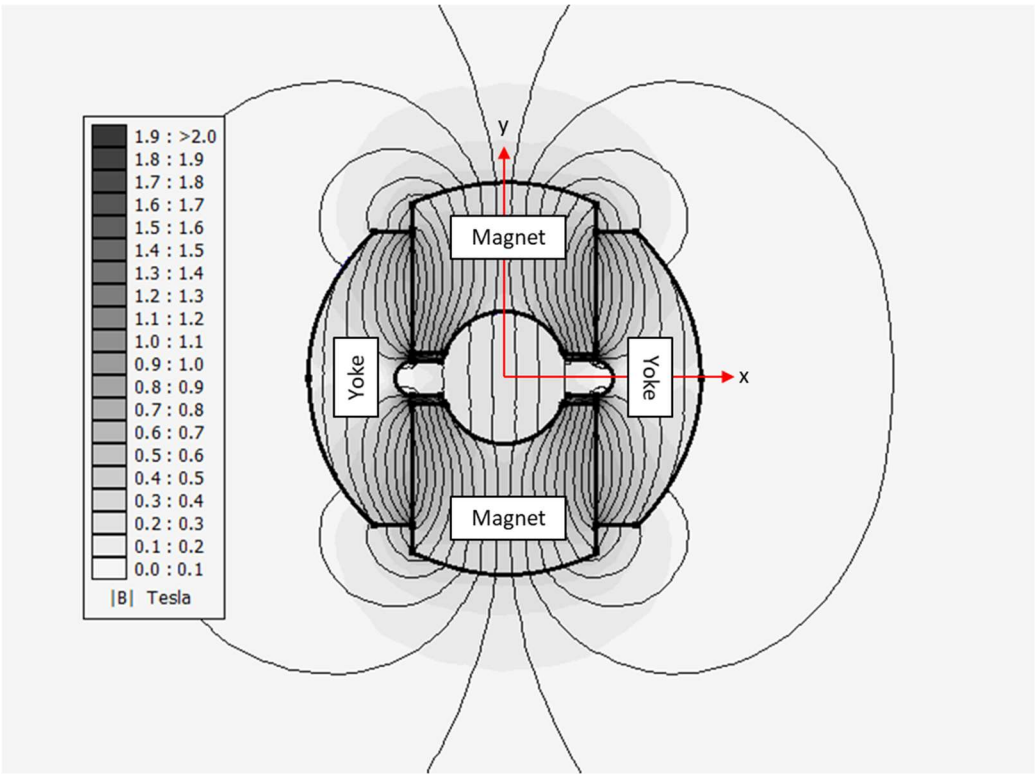

Figure 30 – A two-dimensional FEA model showing the boundary construction and calculated magnetic flux distribution.

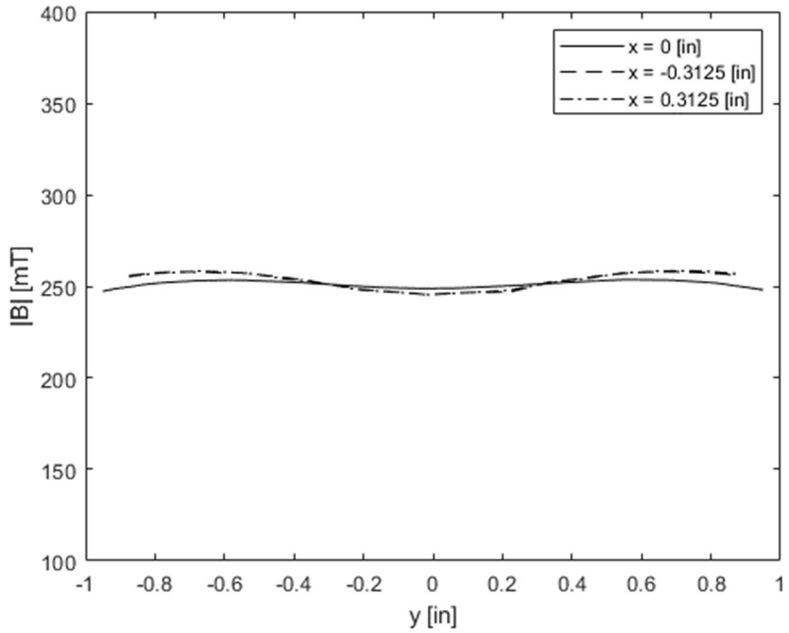

Figure 31 – Vertical cuts from FEA analysis at 0-inches and ±0.3125-inches. The resulting flux density is roughly uniform across the conduit with a nominal magnitude of about 260 mT.

Next, the average magnetic field strength from Figure 30 and Figure 31 were used with the EMFM theory in Equation 7 through Equation 10 to calculate the induced signal as a function of flowrate. Figure 32 plots

the theoretical voltage output as a function of flowrate for three temperatures. These curves estimate that the expected signal will be approximately 1 mV for every 3 GPM of flow at 400 C. Additionally, this analysis estimates that the lowest measurable flowrate will be roughly 10 GPM at 4 mV and 250 C.

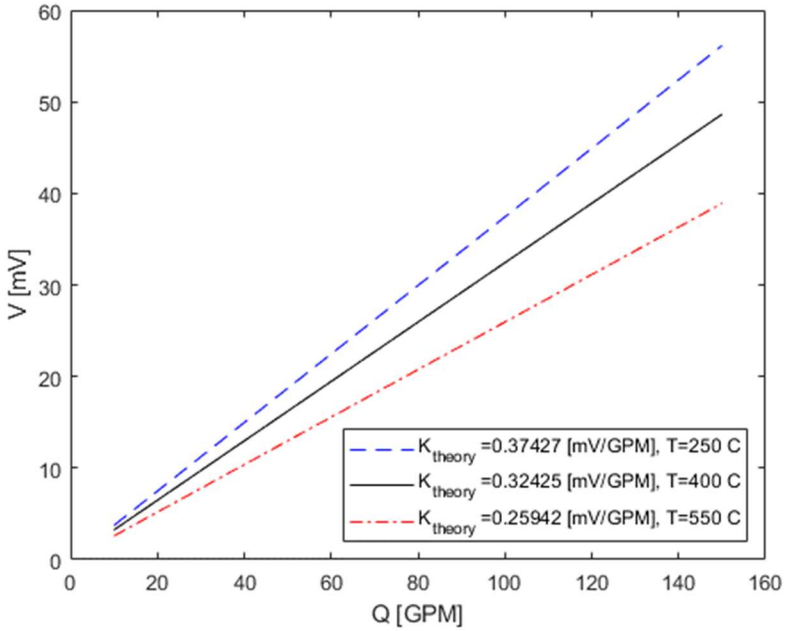

Figure 32 – Theoretical EMFM signal output as a function of flowrate and temperature.

4 Conclusions and Path Forward

F-STAr is a METL test article providing high flowrate sensor, component, or flow structure testing capabilities. The test article includes a high-capacity pump capable of providing a nominal flowrate of 120 GPM; a versatile support structure which can accommodate a wide array of test sections, instrumentation, components, fluid studies, and more; and lastly a heating and cooling system to help experimenters control fluid conditions. These main components are built from and mounted to standard ANSI flange patterns which gives the experimenter flexibility during the design process to substitute components as needed.

In the initial deployment, F-STAr will aid in developing and testing SFR flow sensors such as ECFS's. Therefore, the pump has been sized to provide realistic, single fuel subassembly flowrates. Additionally, the test article is equipped with two test sections; the first test section represents a "Full-Scaled" fuel handling socket; the second test section represents a "Pseudo-Scaled" array of fuel handling sockets. These test sections model nominal socket dimensions identified in literature of several SFR designs including the ABTR, AFR, ALMR, FASTER, and PRISM.

While initially configured to study flow sensors, F-STAr can also accommodate other experimental needs. For example, the test article could be outfitted with a test section that includes a scaled fluidic diode or a hydrodynamic bearing study. Other setups include fluid studies such as thermal structure studies of thermal striping or pool-jet phenomena. Overall, F-STAr is designed to be a flexible facility capable of providing experimenters with relatively large sodium flowrates.

In total, this report covered the current status of F-STAr. This included a general overview of the test article and the interfaces between each component. Then, each of the main components were describe in detail. These descriptions included the 120-GPM pump, support structure and test sections, 5-kW heater, 2-kW cooler and cooling system, and finally the submersible flowmeter. At the time of this writing, all major design work has been completed and the first drafts of engineering drawings are nearly complete. Additionally, several components are currently in production. These include the high-temperature pump, 5 kW heater, as well as the energized C-rings for the pump and test section components.

Therefore, the status of F-STAr has transitioned from the final design phase and into a procurement and manufacturing phase. Below are bullet points of the near-term steps that will be completed.

- Compile an engineering drawing package with a manufacturing specifications sheet.
- Send out drawing package for an RFQ and select a vendor or multiple vendors.
- Manufacture and inspect F-STAr components.
- Mock-up F-STAr in water for quantification of pump, heater, and cooler performance.

Additionally, more work will be completed studying and developing a prototype ECFS that will be initially installed in F-STAr. Figure 33 show a sketch of a hypothetical ECFS configuration to be investigated during the F-STAr work. The sensor below is a five-coil configuration probe-type design with a solid bobbin, which reflects some aspects specified in the RDT C4-7T sensor and the sensors used in the Fast Flux Test Facility. Currently, analytical and numerical models are being investigated to help aid in the sensor designs. Important parameters include the driving frequency, driver and receiver coil geometry, coil radial thicknesses, bobbin material, and sheath thickness. Other challenges which will be investigated include temperature compensations and sensor calibrations.

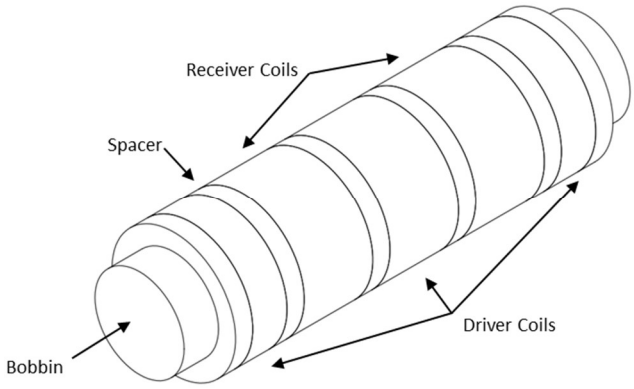

Figure 33 – Sketch of a hypothetical ECFS configuration to be studied in F-STAr.

Below are bullets points of the near-term steps that will be competed for ECFS development.

- Complete literature review of ECFS's, identifying the state-of-the-art and challenging for cutting edge sensors.
- Review and implement published analytical ECFS theory and/or developed ECFS numerical models in a physics modeling software such as ANSYS/FLUENT or COMSOL.
- Analyze and construct prototype sensors based on RDT C4-7T and in-house designs.

5 Acknowledgements

The authors would like to acknowledge METL team member Daniel Andujar for all the hard work and dedication to constructing, maintaining, and operating the facility. This work is funded by the U.S. Department of Energy Office of Nuclear Energy's Advanced Reactor Technologies program. A special acknowledgement of thanks goes to Mr. Brian Robinson, Fast Reactor Program Manager for the DOE-NE ART program and to Dr. Robert Hill, the National Technical Director for Fast Reactors for the DOE-NE ART program for their consistent support of the Mechanisms Engineering Test Loop and its associated experiments, including F-STAr.

6 References

[1] M. El-Wakil, Nuclear Energy Conversion, Scranton, Pennsylvania: Intext Education Publishers, 1971, p. 330.

[2] Argonne National Laboratory, "Advanced Burner Reactor 1000 MWth Reference Concept," Lemont, 2007. ANL-AFCI-202.

[3] Argonne National Laboratory, "Advanced Fast Reactor - 100 (AFR-100) Report for the Technical Review Panel," Lemont, 2014. ANL-ARC-288.

[4] GE Nuclear Energy, "ALMR Summary Plant Design Description," San Jose, 1993.

[5] Argonne National Laboratory, "FASTER Test Reactor Preconceptual Design Report," Lemont, 2016. ANL.ART-86.

[6] General Electric, "PRISM Preliminary Safety Information Document," San Jose, 1987.

[7] M. Weathered, D. Kultgen, E. Kent, C. Grandy, T. Sumner, A. Moisseytsev and T. Kim, "Thermal Hydraulic Experimental Test Article - Status Report for FY2019 Rev. 1," Lemont, 2019. ANL-ART-176 Rev. 1./ANL-METL-21.

[8] M. Weathered, D. Kultgen, E. Kent, C. Grandy, T. Sumner, A. Moisseytsev, T. Kim, "Thermal Hyrdaulic Experimental Test Article - Status Report FY2020," Lemont, 2020. ANL-ART-211 / ANL-METL-25.

[9] I. Idelchik, "Reistance to Flow Through Pipe Fittings and Labyrinth Seals," in *Handbook of Hydraulic Resistance*, 3rd ed., Mumbai, Jaico Publishing House, 2008, pp. 541-586.

[10] R. Campana, E. Diehl and R. Faught, "Components," in *Liquid Metal Handbook*, H. Grantz, Ed., The Atomic Energy Commission, 1955.

[11] H. Elrod and R. Fouse, "An investigation of electromagnet flowmeters," *Transactions of the American Society of Mechanical Engineers,* vol. 74, 1952.

[12] W. Gray, "Magnetic Flowmeter Calibration Results (KAPL-613)," 1951.

[13] J. Shercliff, The Theory of Electromagnetic Flow-Measurement, Cambridge University Press, 1962.

[14] W. C. Gray and E. Astley, "Liquid metal magnetic flowmeters," *Journal of the Instrument Society of America,* vol. 1, pp. 15-23, 1954.

[15] J. Mausteller, F. Tepper and S. Rodgers, Alkali Metal Handling and Systems Operating Techniques, Gordon and Breach, 1968.

[16] U. A. E. Commission, "Permanent Magnet Flowmeter for Liquid Metal Piping Systems (Technical Report RDT C 4-5T)," 1971.

[17] L. G. Vasil'yev and A. I. Kozhainov, "Magnetohydrodynamics in Marine Engineering," 1967.

[18] S. Kim and C. Doose, "Temperature compensation of NdFeB permanent magnets," 1998.

Nuclear Science and Engineering Division
Argonne National Laboratory
9700 South Cass Avenue
Argonne, IL 60439

www.anl.gov

Argonne National Laboratory is a U.S. Department of Energy laboratory managed by UChicago Argonne, LLC